European Radiology
https://doi.org/10.1007/s00330-023-09589-x

European Radiology
EUROPEAN SOCIETY OF RADIOLOGY

CHEST

Radiomics analysis of lung CT for multidrug resistance prediction in active tuberculosis: a multicentre study

Ye Li[1] · Zexuan Xu[1] · Xinna Lv[1] · Chenghai Li[1] · Wei He[1] · Yan Lv[1] · Dailun Hou[1]

Received: 22 November 2022 / Revised: 21 February 2023 / Accepted: 28 February 2023

Abstract

Objectives Multidrug-resistant TB (MDR-TB) is a severe burden and public health threat worldwide. This study aimed to develop a radiomics model based on the tree-in-bud (TIB) sign and nodules and validate its predictive performance for MDR-TB.

Methods We retrospectively recruited 454 patients with proven active TB from two hospitals and classified them into three training and testing cohorts: TIB ($n = 295$, 102), nodules ($n = 302$, 97), and their combination ($n = 261$, 81). Radiomics features relating to TIB and nodules were separately extracted. The maximal information coefficient and recursive feature elimination were used to select informative features per the two signs. Two radiomics models were constructed to predict MDR-TB using a random forest classifier. Then, a combined model was built incorporating radiomics features based on these two signs. The capability of the models in the combined training and testing cohorts was validated with ROC curves.

Results Sixteen features were extracted from TIB and 15 from nodules. The AUCs of the combined model were slightly higher than those of the TIB model in the combined training cohort (0.911 versus 0.877, $p > 0.05$) and testing cohort (0.820 versus 0.786, $p < 0.05$) and similar to the performance of the nodules model in the combined training cohort (0.911 versus 0.933, $p > 0.05$) and testing cohort (0.820 versus 0.855, $p > 0.05$).

Conclusions The CT-based radiomics models hold promise for use as a non-invasive tool in the prediction of MDR-TB.

Clinical relevance statement Our study revealed that complementary information regarding MDR-TB can be provided by radiomics based on the TIB sign and nodules. The proposed radiomics models may be new markers to predict MDR in active TB patients.

Key Points

- *This is the first study to build, validate, and apply radiomics based on tree-in-bud sign and nodules for the prediction of MDR-TB.*
- *The radiomics model showed a favorable performance for the identification of MDR-TB.*
- *The combined model holds potential to be used as a diagnostic tool in routine clinical practice.*

Keywords Pulmonary tuberculosis · Drug resistance · Radiomics · Machine learning

Abbreviations

AUC	Area under the ROC curve
CT	Computed tomography
DCA	Decision curve analysis
DST	Drug-sensitive test
DS-TB	Drug-sensitive TB
GLCM	Gray level co-occurrence matrix
GLDM	Gray level dependence matrix
GLRLM	Gray level run length matrix
GLSZM	Gray level size zone matrix
ICC	Intraclass correlation coefficient
MDR-TB	Multidrug-resistant TB
MIC	Maximal information coefficient
NGTDM	Neighboring gray tone difference matrix
RFC	Random forest classifier
RFE	Recursive feature elimination
ROC	Receiver operator characteristic
ROIs	Regions of interest
SMOTE	Synthetic minority oversampling technique
TB	Tuberculosis
TIB	Tree-in-bud

✉ Dailun Hou
hou.dl@mail.ccmu.edu.cn

[1] Department of Radiology, Beijing Chest Hospital, Capital Medical University, Beijing 101149, China

Published online: 01 April 2023

Introduction

Tuberculosis (TB) is a communicable disease that is a major cause of ill health and one of the leading causes of death globally [1]. TB was the top cause of death from a single infectious agent until the coronavirus pandemic [1]. In addition, multidrug-resistant TB (MDR-TB) is still a severe burden worldwide and continues to be a public health threat [2]. MDR-TB refers to resistance to isoniazid and rifampicin, which are otherwise the two most effective first-line drugs. Approximately 3–4% of people are diagnosed with TB for the first time and have MDR-TB, and approximately 18–21% have previously been treated for TB [3]. However, 95% or more of MDR-TB cases have already occurred before diagnosis by passive case finding [4]. Microbiologic culture and sputum smear microscopy are necessary tests for the diagnosis of TB [5]. The predictive value and sensitivity of using sputum as the sample are poor, but using culture isolates always means that results will be available only after 4–8 weeks [1]. Hence, the early identification of patients with MDR-TB will substantially reduce the burden of TB.

Alongside microbiologic culture and sputum, chest computed tomography (CT) is an essential screening method for detecting TB [6]. The most frequent abnormal CT pattern of active TB is the tree-in-bud (TIB) sign. The TIB sign is the constellation of small centrilobular nodules and concomitant branching opacities, which mimics the branching pattern of a budding tree [7]. TIB is observed in approximately 72% of active TB cases [8]. Nodules are also commonly seen in TB patients, and TB is a unique characteristic of benign lung nodules due their high prevalence in TB patients [9]. Several previous studies have shown that multiple cavities, the TIB sign, and nodules are common in MDR-TB [10–12]. However, these prior studies were heterogeneous and non-quantitative, and few quantitative studies have focused on the TIB sign and nodules.

Radiomics is an emerging and non-invasive approach that can extract high-throughput quantitative features from medical images and convert the information into mineable databases [13]. Currently, radiomics is widely used in the differentiation of benign from malignant lesions, in the prediction of disease-free survival, and for diagnostic and prognostic assessments [14]. However, there have been few studies on radiomics analysis based on active TB for MDR-TB prediction.

We hypothesized that the differences between drug-sensitive TB (DS-TB) and MDR-TB could be captured by CT scans, reflected in spatial density patterns, and identified by radiomics. Therefore, the aim of this study was to develop a predictive model by CT radiomics features and to validate the predictive value of the model to distinguish DS-TB from MDR-TB.

Materials and methods

Participants

We retrospectively collected lung CT data from patients in two hospitals from December 2015 to March 2022. The institutional ethics committee approved all the data in the study for retrospective analysis and waived the demand for informed consent.

The enrolled patients met the following inclusion criteria: (a) culture, sputum microscopy, or polymerase chain reaction test to confirm TB; (b) drug susceptibility test (DST) results for *M. tuberculosis* to distinguish DS-TB from MDR-TB; (c) typical imaging findings, whether TIB sign or nodules indicative of TB; and (d) performance of all CT scans before the TB diagnosis. The exclusion criteria were as follows: (a) image artifacts or incomplete clinical information; (b) a history of other pulmonary diseases such as lung cancer or COPD; or (c) diabetes or HIV seropositivity.

Finally, we recruited 336 patients, which included 302 patients with nodules and 295 patients with the TIB sign, as training cohorts 1 and 2. There were 261 patients with these two signs as the combined training cohort in hospital 1 from December 2015 to January 2022. In addition, testing cohorts from hospital 2, including 97 patients with nodules, 102 patients with the TIB sign, and 81 patients with these two signs, were subsequently enrolled from August 2017 to March 2022. Detailed information on the patient recruitment flowchart is shown in Fig. 1.

CT examination

All lung CT scans were performed using a Revolution CT or Light Speed VCT (GE Healthcare). The scanning included imaging from the thoracic inlet to the bilateral adrenal glands with deep inspiration breath-hold. The scanning parameters were as follows: tube voltage, 120 kV; automatic tube current modulation; detector collimation, 64×0.625 mm; rotation time, 500 ms; and pitch, 1.375. The image reconstruction parameters were as follows: slice thickness, 1.25 mm; increment, 1.25 mm; field of view, 15 cm; and matrix, 512×512. Then, the reconstructed images were transferred to 3D slicer (http://www.slicer.org) for radiomics analysis.

Lesion segmentation

The TIB sign was defined as multiple areas of centrilobular nodules with a linear branching pattern that resembles a budding tree [7]. Nodule refers to a rounded or irregular opacity, well or poorly defined, measuring up to 3 cm in diameter [15]. Regions of interest (ROIs) were separately drawn to segment TIB and nodules, manually contoured

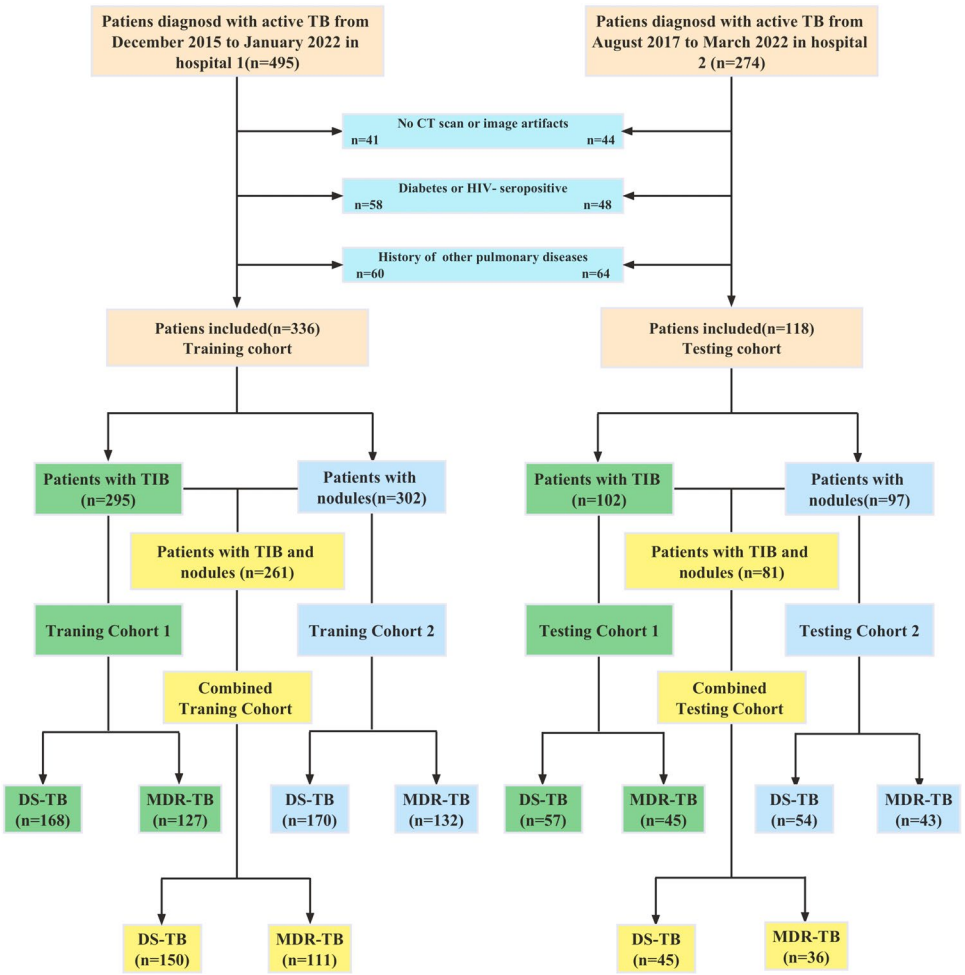

Fig. 1 Flowchart of patient selection

including the whole surface of the lesions layer by layer, including circumambient satellite lesions in lung windows. The ROIs were drawn by an experienced chest radiologist and confirmed by an independent radiologist with 10 years of experience in lung CT. The two radiologists were blinded to the DST results.

Radiomics feature extraction

The radiomics features were separately extracted from TIB and nodules. Preprocessing and detailed information about the radiomics features is provided in the Supplementary Material and PyRadiomics official documentation. (https://pyradiomics.readthedocs.io/en/latest/features.html).

Feature selection

First, 30 patients with the TIB sign or nodules were randomly selected to calculate the intraclass correlation coefficient (ICC) as previously reported [16]. Another radiologist with 8 years of experience segmented the lesions of these patients. The aim of this study was to establish a resegmentation dataset for evaluating the interreader reproducibility of radiomics features. Features with ICC > 0.80 were considered to be highly reproducible and were retained. Given the unbalanced nature of the training dataset, the synthetic minority oversampling technique (SMOTE) was used on the training cohort to handle the imbalance between DS-TB patients and MDR-TB patients with the purpose of avoiding bias towards majority class cases and achieving a high classification rate [17]. To determine representative features for generalizing and optimizing the model, we used the maximal information coefficient (MIC) to identify important relationships in datasets and characterize them [18]. As a result, we separately chose the top 200 relevant features from the TIB sign and nodules in training cohort 1 and 2 according to the MIC values. Then, we used the recursive feature elimination (RFE) method to extract the most important features of prediction by finding a high correlation between specific features and labels. The RFE algorithm is very popular due to its effectiveness in selecting features in training datasets relevant to predicting target variables and eliminating weak features [19]. Tenfold cross-validation was utilized to avoid overfitting. We separately plotted the

number of features in the dataset along with a cross-validated score and visualized the selected features.

Model construction and application

The random forest classifier (RFC) is a method that possesses high variance-bias trade-off capability, so RFC was used to construct the prediction models [20]. In training cohort 1, the selected radiomics features from the TIB sign were trained by using the RFC method. Then, radiomics features based on the nodules were selected to build a model in training cohort 2. Finally, we built and applied three radiomics models in the combined training cohort, which included a TIB model, nodules model, and combined model with the combination of all radiomics features based on the two typical lesions. These models were all trained and validated on the three training cohorts, which were randomly divided into parts at a ratio of 7:3 using tenfold cross-validation. Finally, we separately selected the best model of all models and tested it on the corresponding cohort of three external testing cohorts. Feature selections and model construction were carried out by the Python Scikit-learn package (version 3.8, Scikit-learn Version 0. 21, http://scikit-learn.org/). Our radiomics-based machine learning workflow pipeline is shown in Fig. 2.

Statistical analysis

Statistical analysis was performed with SPSS software (version 26) and the Python Scikit-learn package. Qualitative variables (sex) are presented as frequencies. The chi-square test was used to analyze differences between sexes, and a *t* test was used to analyze age. Receiver operator characteristic (ROC) curves, which were used to calculate the area under the ROC curve (AUC), were used to evaluate the performance of all models in both cohorts. The DeLong test was used to analyze the AUCs of three radiomics models in the combined cohort and evaluate whether overfitting

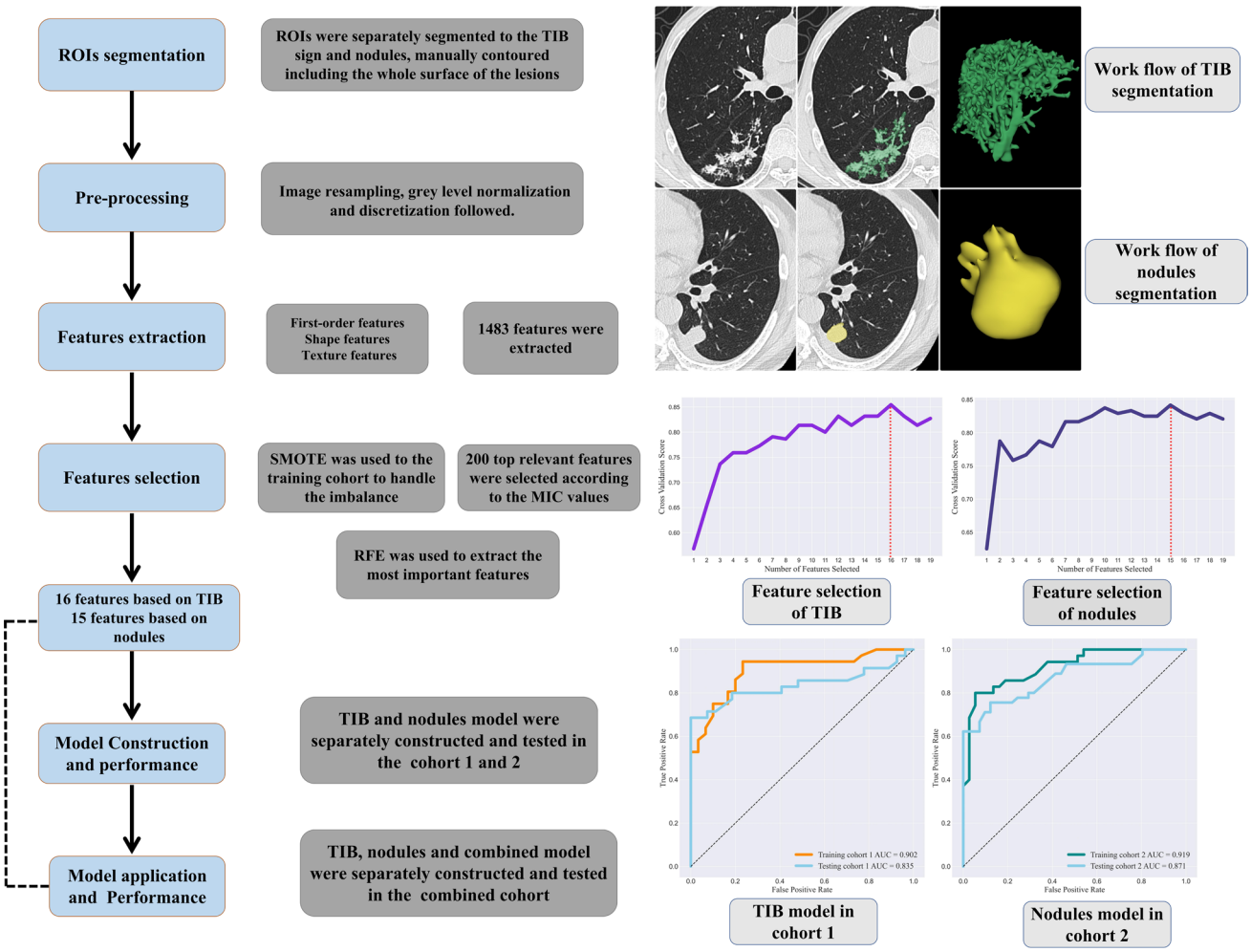

Fig. 2 The workflow of this study. The full line represented the process of the radiomics features selection and model construction in cohort 1 and 2; the dotted line represented the process of the model construction and application the combined cohort

occurred. Then, we used decision curve analysis (DCA) to determine the clinical usefulness of the TIB model, nodule model, and combined model by calculating the net benefits at different threshold probabilities in the combined training and testing cohort. Briefly, the net benefit was equivalent to the proportion of net true positives. The accuracy, precision (positive predictive value), recall (sensitivity), and F1 score were calculated. The F1 score is the harmonic average of the precision and recall, ranging from 0 to 1. Statistical tests were conducted with $p < 0.05$ as an indicator of statistical significance.

Results

Clinical characteristics of the patients

There were significant differences in age between MDR-TB patients and DS-TB patients in all the training cohorts ($p < 0.05$), whereas age was not significantly different between the two groups in any testing cohorts. In addition, the remaining clinical characteristics (sex) were not significantly different between MDR-TB and DS-TB patients in any cohort. Details of the basic characteristics of all the training and testing cohorts are summarized in Table 1.

Radiomics feature selection and model construction

We identified 200 top relevant features according to the MIC values. Finally, 16 features extracted from the TIB sign and 15 features extracted from nodules were selected to build the model because of the highest cross-validated score. The normalized importance of the selected features is separately shown in Fig. 3. In addition, detailed values and distributions of these features are separately presented by the violin plot in Fig. 4. The radiomics model based on the TIB showed a favorable discriminatory ability in training cohort 1 with an AUC of 0.902 (95% CI, 0.836 to 0.959), which was confirmed in testing cohort 1 with an AUC of 0.835 (95% CI, 0.739 to 0.922). In addition, the radiomics model based on the nodules also showed good performance in training and testing cohort 2, with AUCs of 0.919 (95% CI, 0.867 to 0.964) and 0.871 (95% CI, 0.810 to 0.929), respectively.

Model construction and evaluation in combined cohorts

The 16 radiomics features selected from TIB and 15 radiomics features selected from nodules were separately comprised of TIB model, nodules model, and combined model in combined cohorts. The ROC curve AUCs of these three models in the combined training and testing cohorts are shown in Fig. 5. The combined model showed the best performance

Table 1 Basic clinical characteristics of DS-TB and MDR-TB in training and testing cohorts

Characteristic	Patients with TIB sign						Patients with nodules						Patients with TIB sign and nodules					
	Training cohort ($n = 295$)		p-value	Testing cohort ($n = 102$)		p-value	Training cohort ($n = 302$)		p-value	Testing cohort ($n = 97$)		p-value	Training cohort ($n = 261$)		p-value	Testing cohort ($n = 81$)		p-value
	DS-TB ($n = 168$)	MDR-TB ($n = 127$)		DS-TB ($n = 57$)	MDR-TB ($n = 45$)		DS-TB ($n = 170$)	MDR-TB ($n = 132$)		DS-TB ($n = 54$)	MDR-TB ($n = 43$)		DS-TB ($n = 150$)	MDR-TB ($n = 111$)		DS-TB ($n = 45$)	MDR-TB ($n = 36$)	
Gender																		
Male	87	67	0.869	27	25	0.411	91	75	0.569	29	24	0.836	78	59	0.854	26	23	0.576
Female	81	60		30	20		79	57		25	19		72	52		19	13	
Age (mean±SD years)	39.01 ± 17.59	33.68 ± 13.23	0.040*	36.66 ± 15.05	36.47 ± 12.23	0.966	38.18 ± 15.44	34.27 ± 13.70	0.033*	36.27 ± 14.19	36.33 ± 14.28	0.984	38.08 ± 16.83	33.33 ± 12.31	0.038*	37.61 ± 15.78	36.00 ± 14.77	0. 621

Differences were assessed by *t* test or chi-square test. *SD*, standard deviation. *$p < 0.05$

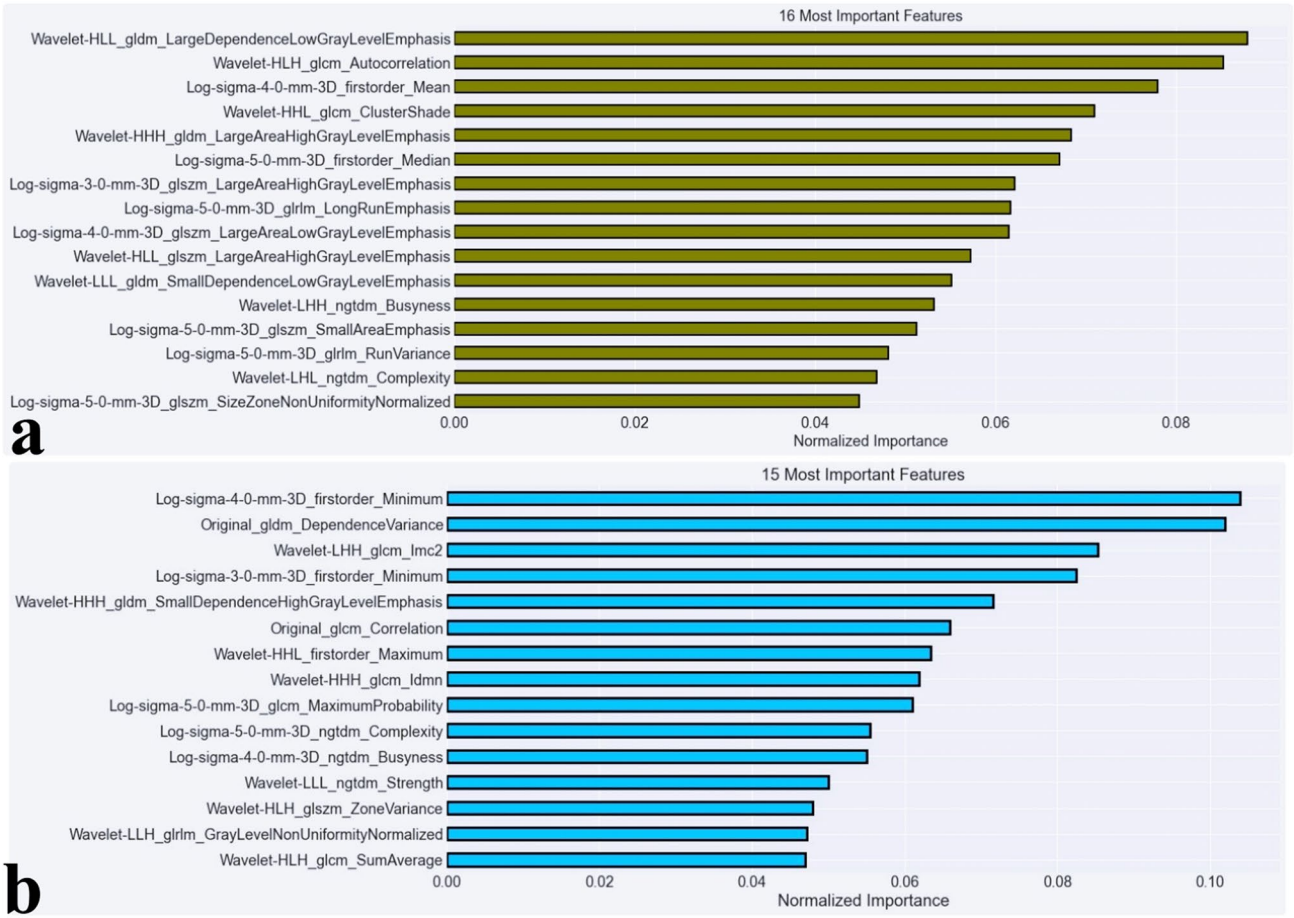

Fig. 3 The 16 radiomics features based on TIB (**a**) and 15 radiomics features based on nodules (**b**) with the highest normalized importance were selected and included

for discriminating multidrug resistance (MDR), with AUCs and F1 scores of 0.911 (95% CI, 0.838 to 0.974) and 0.833, and 0.820 (95% CI, 0.659 to 0.955) and 0.832, respectively. The AUCs and F1 scores of the TIB model were 0.877 (95% CI, 0.871 to 0.982) and 0.786 (95% CI, 0.640 to 0.905) and 0.817 and 0.789 in the two cohorts, respectively. The nodules model also showed excellent discriminatory ability in the combined training cohort, with an AUC of 0.933 (95% CI, 0.871 to 0.982) and an F1 score of 0.833, which was confirmed in the testing cohort with an AUC of 0.855 (95% CI, 0.714 to 0.973) and an F1 score of 0.778. In addition, there was no significant difference between the combined model and nodules model in the combined training ($p = 0.538$) and testing ($p = 0.504$) cohorts. More specifically, the AUCs of the combined model were not significantly different from those of the TIB model in the training cohort ($p = 0.504$), and there were significant differences between the two models in the testing cohort ($p = 0.038$). Finally, the AUCs between the TIB model and nodules model were not significantly different between the two cohorts ($p = 0.313$ and 0.054). The DCA curves, as presented in Fig. 6, showed that all three models, including the TIB model, nodules model, and combined model, would offer net benefits over the "treat-all" or "treat-none" scheme within a certain range of thresholds in the combined training cohort. Similar results were found in the testing cohort. The accuracy, precision, recall, and F1 score of all three models in the combined training and testing cohorts are summarized in Table 2.

Discussion

In the present study, we developed and validated CT-based radiomics models based on TIB and nodules for differentiating DS-TB from MDR-TB. These radiomics models hold the potential to facilitate a non-invasive individualized identification of MDR in TB patients. The combined model showed the best predictive performance, and the performance was higher than that of the TIB model and similar to that of the nodules model.

This study collected data on the basic clinical characteristics of all patients. The analysis showed that the age of

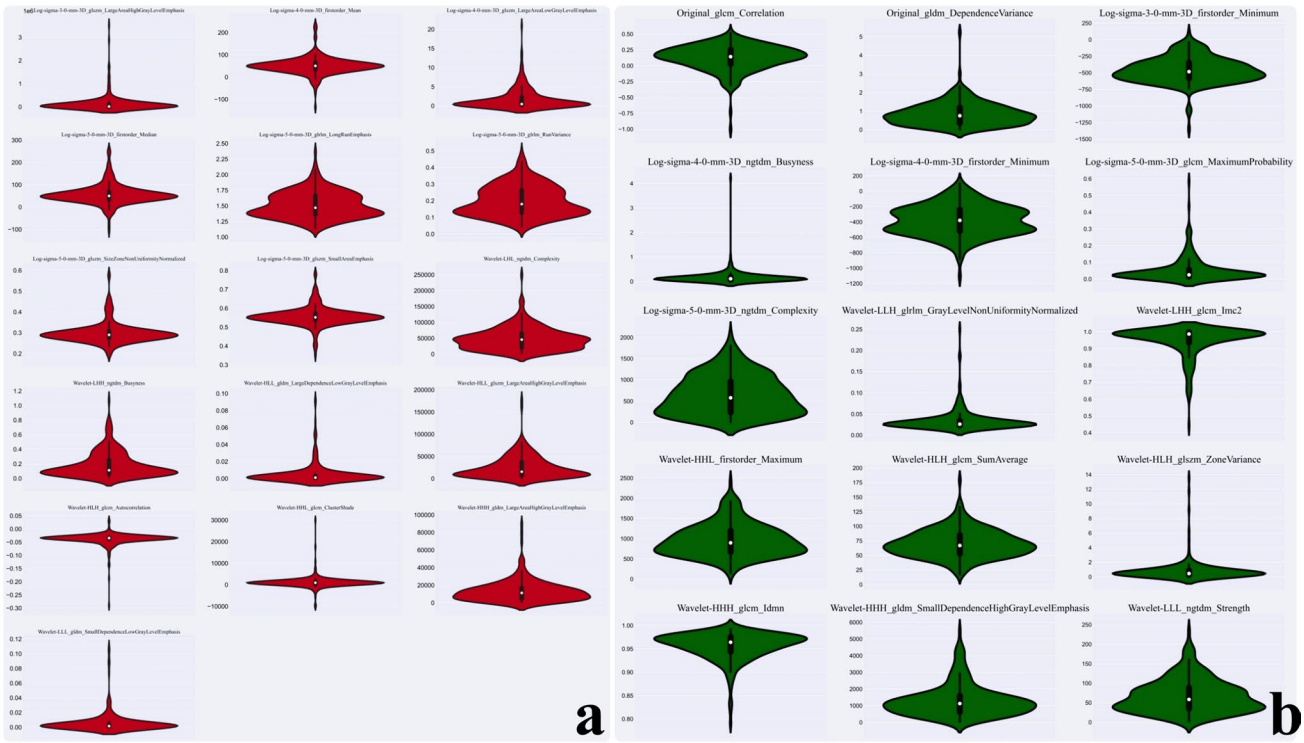

Fig. 4 These violin plots show the detailed values and distributions of 16 features based on TIB (**a**) and 15 features based on nodules (**b**)

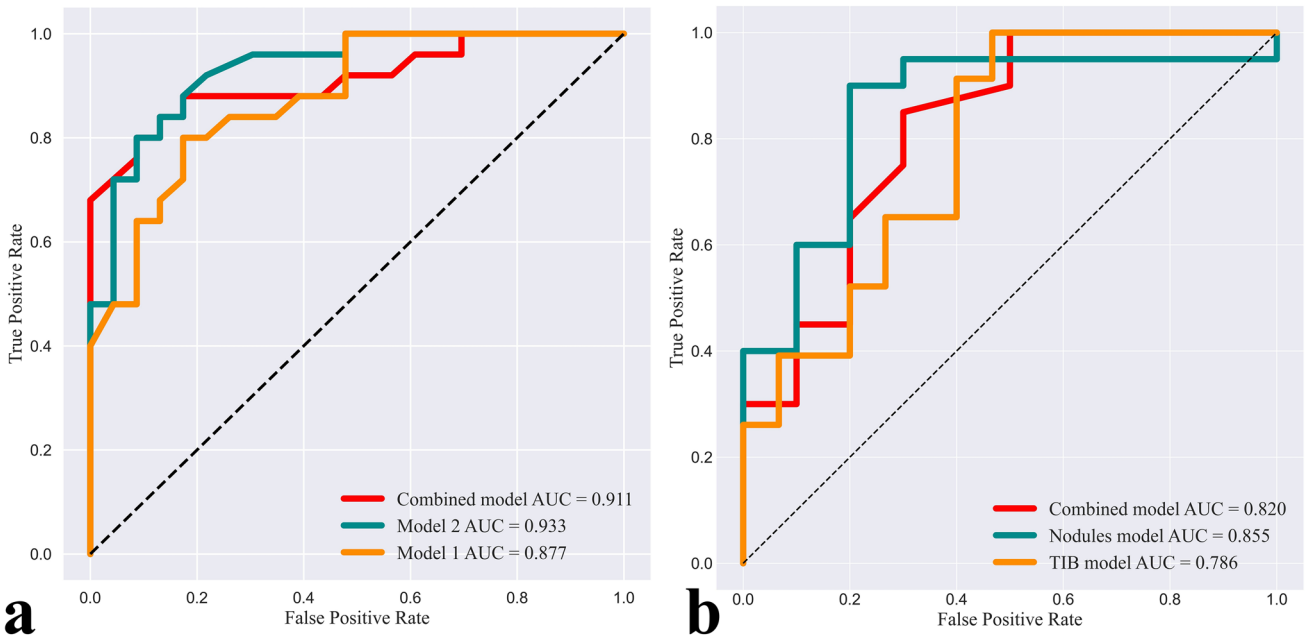

Fig. 5 ROC curves of the TIB, nodules, and combined model. **a** Training cohort. **b** Testing cohort

MDR-TB patients was significantly different from that of DS-TB patients in all training cohorts. However, there was no significant difference in age between the two groups in any testing cohort. This is consistent with the findings of a previous study finding that MDR-TB patients were younger than DS-TB patients [21]. In addition, there was

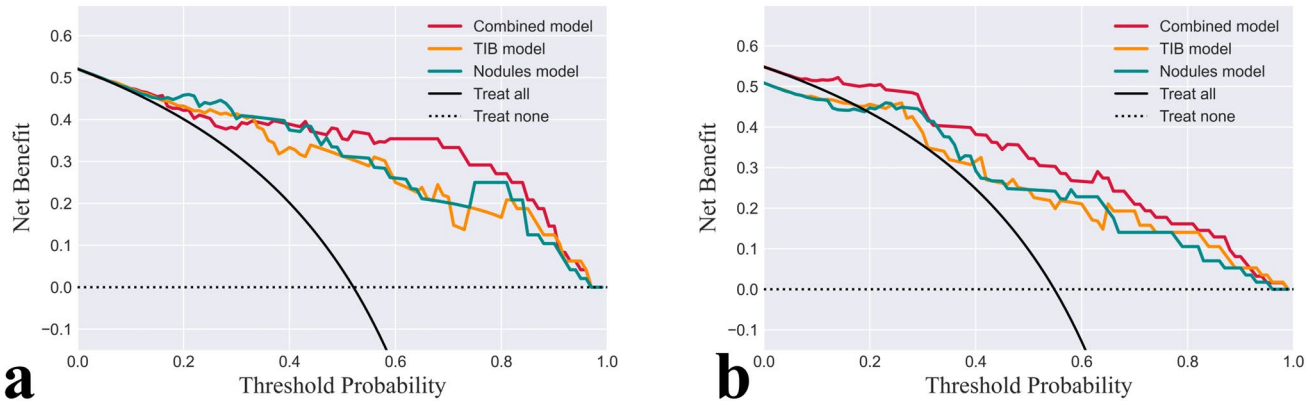

Fig. 6 DCA for the TIB, nodules, and combined model in the training cohort (**a**) and the testing cohort (**b**). The net benefit versus the threshold probability is plotted. Black line represents the assumption that all patients were MDR-TB. Dotted line represents the assumption that all patients were DS-TB. The *x*-axis shows the threshold probability. The *y*-axis shows the net benefit. A model is only clinically useful if it has a higher net benefit than the default treat-all (all cases were MDR-TB) and treat-none (none of the cases was MDR-TB) strategies. It is clear from the graph that these three models are superior to either treat-all or none strategy within certain ranges of risk threshold

Table 2 Predictive performance of three models in the combined training and testing cohorts

Index	Training cohort			Testing cohort		
	TIB model	Nodules model	Combined model	TIB model	Nodules model	Combined model
AUC	0.877	0.933	0.911	0.786	0.855	0.820
Accuracy	0.803	0.833	0.833	0.758	0.767	0.774
Precision	0.829	0.811	0.870	0.778	0.778	0.889
Recall	0.806	0.857	0.800	0.800	0.778	0.782
F1 score	0.817	0.833	0.833	0.789	0.778	0.832

no difference in sex between MDR-TB and DS-TB patients in any cohorts, which was similar to the results of other studies [21, 22].

TB still poses a severe threat to public health, especially with the increasing incidence of MDR-TB, resulting in difficulty in controlling the epidemic [23]. Acid-fast bacilli or bacterial cultures are accurate bacteria-based detection methods based on bacteria, but are time-consuming. In addition, new gene testing methods are always inconvenient and may be restricted by the laboratory environment [24]. Therefore, it is necessary to develop a non-invasive and user-friendly model focused on the prediction of MDR for TB patients.

The TIB has most commonly been described in TB patients with pulmonary infectious disorders and was the most characteristic but not pathognomonic CT feature of active TB [25]. It always reflects the presence of endobronchial spread, caseous necrosis, and granulomatous inflammation filling surrounding respiratory bronchioles and alveolar ducts [26]. It was reported that large nodules, including ground-glass opacities, were more frequently observed in MDR-TB patients [12]. However, these signs can only be considered to be a marker of the active pathological process rather than being MDR-TB specific. Several studies have confirmed that only imaging findings of MDR-TB do not differ from those of DS-TB [12, 27]. Even though MDR-TB patients generally tend to have more extensive lesions, are more likely to have bilateral lesions, have large nodules, and have a larger scope of the TIB sign, these signs are insufficient to discriminate MDR-TB from DS-TB [12]. Thus, it is essential to explore the specific differences between MDR-TB and DS-TB using quantitative analysis, and radiomics seems promising in this regard.

Numerous prior studies have described the utility of radiomics approaches to discriminate solitary TB nodules from lung adenocarcinoma. A deep learning–based nomogram using radiomics based on CT and clinical factors was developed and validated to differentiate two diseases, obtaining an AUC of 0.906 in the external validation cohort [28]. In addition, Hu et al established a radiomics model containing a set of nine [^{18}F]FDG PET/CT radiomics features from 235 patients, which achieved an encouraging predictive performance (AUC = 0.889) [29]. Another similar study utilized a radiomics nomogram integrating the radiomics score of features selected from [^{18}F]FDG PET/CT, with an AUC of 0.93 in the validation cohort [30]. Few studies have focused on

the identification of MDR-TB based on radiomics. A recent publication established a radiomics model to predict MDR in cavitary TB with severe transmission and poor treatment outcome, and timely identification of cavitary MDR-TB can adjust therapies and improve prognosis [31]. The current study focused on the two most frequent signs of active TB to differentiate MDR-TB from DS-TB. Its advantage was mainly the timely identification of MDR-TB before TB progression, especially when patients had only one or both of the typical signs, and it could lead to a high success rate and reduced recurrence in patients. To our knowledge, no published study has focused on radiomics based on the TIB sign and nodules of active TB, as was done in this study. As a result, we attempted to further solve this most relevant clinical question to differentiate MDR-TB from DS-TB based on the most frequent CT signs of active TB.

In our study, we proposed three radiomics models using RFC that involved 16 radiomics features based on the TIB sign and 15 radiomics features based on the nodules to predict MDR-TB, and these models all achieved good performance. These radiomics models had several advantages. First, there was a relatively high AUC (0.911 vs. 0.820) in the combined model, and the predictive power of the single radiomics model was robust enough even if the AUC of the nodules model was slightly higher than that of the combined model (0.933 vs. 0.911). In addition, these models, especially the combined model and nodules model, showed good performance according to the F1 score, which could provide a more realistic assessment for radiomics models. Second, 1483 radiomics features were separately extracted from the TIB sign and nodules, which included first-order features, shape-based (3D, 2D) features, GLCM features, GLRLM features, GLSZM features, GLDM features, and NGTDM features. Then, we took two steps, including MIC and RFE, to eliminate weak features, and ultimately, 16 features and 15 features were put into the model construction, allowing for a credible result. Third, we retrospectively gathered two cohorts (training and testing) that focused on the TIB sign and nodules, respectively, to select features and construct models. Then, we applied these two models in the combined cohorts (training and testing) and established a combined model to guarantee good stability and generalizability in clinical practice. Above all, these three models, especially the combined model in the current study, yielded an excellent performance for the distinction of MDR-TB and could offer net benefits over all the "treat-all" or "treat-none" strategies within a certain threshold probability.

The study had several limitations. First, the current study was a retrospective analysis with a small sample size. However, inherent selection bias may exist. Second, we focused only on the MDR classification of active TB patients with the TIB sign or nodules, although these signs were frequent in TB patients. The role of radiomics in the prediction of patients without these signs was not investigated, which merits further studies. Third, limited clinical information was involved in the present study, and the models that we established did not include any clinical information. Fourth, considering the small sample size of the testing cohort, future studies should concentrate on prospective studies to increase generalizability.

In conclusion, we developed three CT image-based radiomics models for the identification of MDR-TB patients. These models were separately trained and tested in three cohorts, and these models, especially the combined model and nodules model, showed excellent performance. Our study may potentially aid in early MDR-TB characterization by integrating the multidisciplinary approach currently based on radiomics and can be used as a non-invasive auxiliary tool.

Supplementary Information The online version contains supplementary material available at https://doi.org/10.1007/s00330-023-09589-x.

Acknowledgements This research was funded by the Beijing Hospitals Authority Clinical Medicine Development of Special Funding and Beijing Key Clinical Specialty Project (20201214). The funding source provided financial support without any influence on the study design and interpretation of data. We would like to thank our groups from many hospitals for the data collection and interpretation.

Funding This study has received funding from the Beijing Hospitals Authority Clinical Medicine Development of Special Funding (XMLX202146) and Beijing Key Clinical Specialty Project (20201214). The funders had a role in the study design and submitted the paper for publication.

Declarations

Guarantor The scientific guarantor of this publication is Dailun Hou.

Conflict of interest The authors of this manuscript declare no relationships with any companies, whose products or services may be related to the subject matter of the article.

Statistics and biometry No complex statistical methods were necessary for this paper.

Informed consent Written informed consent was waived by the Institutional Review Board.

Ethical approval Institutional Review Board approval was obtained.

Methodology
- retrospective
- diagnostic study
- multicenter study

References

1. Bagcchi S (2023) WHO's Global Tuberculosis Report 2022. Lancet Microbe 4(1):e20
2. Dheda K, Gumbo T, Maartens G et al (2019) The Lancet Respiratory Medicine Commission: 2019 update: epidemiology,

pathogenesis, transmission, diagnosis, and management of multidrug-resistant and incurable tuberculosis. Lancet Respir Med 7(9):820–826
3. Fox GJ, Schaaf HS, Mandalakas A, Chiappini E, Zumla A, Marais BJ (2017) Preventing the spread of multidrug-resistant tuberculosis and protecting contacts of infectious cases. Clin Microbiol Infect 23(3):147–153
4. Dheda K, Gumbo T, Maartens G et al (2017) The epidemiology, pathogenesis, transmission, diagnosis, and management of multidrug-resistant, extensively drug-resistant, and incurable tuberculosis. Lancet Respir Med S2213–2600(17)30079–6. https://doi.org/10.1016/S2213-2600(17)30079-6
5. Shi W, Davies Forsman L, Hu Y et al (2020) Improved treatment outcome of multidrug-resistant tuberculosis with the use of a rapid molecular test to detect drug resistance in China. Int J Infect Dis 96:390–397
6. Skoura E, Zumla A, Bomanji J (2015) Imaging in tuberculosis. Int J Infect Dis 32:87–93
7. Verma N, Chung JH, Mohammed TL (2012) Tree-in-bud sign. J Thorac Imaging 27(2):W27. https://doi.org/10.1097/RTI.0b013e31824643ae
8. Im JG, Itoh H, Shim YS et al (1993) Pulmonary tuberculosis: CT findings–early active disease and sequential change with antituberculous therapy. Radiology 186(3):653–660
9. Bai C, Choi CM, Chu CM et al (2016) Evaluation of pulmonary nodules: clinical practice consensus guidelines for Asia. Chest 150(4):877–893
10. Jihoon C, Yun LH, Soo LK et al (2009) Radiological findings of extensively drug-resistant pulmonary tuberculosis in non-AIDS adults: comparisons with findings of multidrug-resistant and drug-sensitive tuberculosis. Korean J Radiol 10(3):207–216
11. Kim W, Lee KS, Kim HS et al (2016) CT and microbiologic follow-up in primary multidrug-resistant pulmonary tuberculosis. Acta Radiol 57(2):197–204
12. Wáng YXJ, Chung MJ, Skrahin A, Rosenthal A, Gabrielian A, Tartakovsky M (2018) Radiological signs associated with pulmonary multi-drug resistant tuberculosis: an analysis of published evidences. Quant Imaging Med Surg 8(2):161–173
13. Mayerhoefer ME, Materka A, Langs G et al (2020) Introduction to radiomics. J Nucl Med 61(4):488–495
14. Gillies RJ, Kinahan PE, Hricak H (2016) Radiomics: images are more than pictures, they are data. Radiology 278(2):563–577
15. Carlesi E, Orlandi M, Mencarini J et al (2019) How radiology can help pulmonary tuberculosis diagnosis: analysis of 49 patients. Radiol Med 124(9):838–845
16. Koo TK, Li MY (2016) A guideline of selecting and reporting intraclass correlation coefficients for reliability research. J Chiropr Med 15:155–163
17. Nakamura M, Kajiwara Y, Otsuka A, Kimura H (2013) LVQ-SMOTE - learning vector quantization based synthetic minority over-sampling technique for biomedical data. BioData Min 6(1):16. Published 2013 Oct 2. https://doi.org/10.1186/1756-0381-6-16
18. Reshef DN, Reshef YA, Finucane HK et al (2011) Detecting novel associations in large data sets. Science 334(6062):1518–1524
19. Senan EM, Al-Adhaileh MH, Alsaade FW et al (2021) Diagnosis of chronic kidney disease using effective classification algorithms and recursive feature elimination techniques. J Healthc Eng 2021:1004767. https://doi.org/10.1155/2021/1004767
20. Breiman L (2001) Random Forests, machine learning. Springer 45(1):5–32
21. Baya B, Achenbach CJ, Kone B et al (2019) Clinical risk factors associated with multidrug-resistant tuberculosis (MDR-TB) in Mali. Int J Infect Dis 81:149–155
22. Li D, He W, Chen B, Lv P (2017) Primary multidrug-resistant tuberculosis versus drug-sensitive tuberculosis in non-HIV-infected patients: comparisons of CT findings. PLoS One 12(6):e0176354. https://doi.org/10.1371/journal.pone.0176354
23. Lange C, Dheda K, Chesov D, Mandalakas AM, Udwadia Z, Horsburgh CR Jr (2019) Management of drug-resistant tuberculosis. Lancet 394(10202):953–966
24. Liang S, Ma J, Wang G et al (2022) The application of artificial intelligence in the diagnosis and drug resistance prediction of pulmonary tuberculosis. Front Med (Lausanne) 9:935080. https://doi.org/10.3389/fmed.2022.935080
25. Eisenhuber E (2002) The tree-in-bud sign. Radiology 222(3):771–772
26. Hatipoğlu ON, Osma E, Manisali M et al (1996) High resolution computed tomographic findings in pulmonary tuberculosis. Thorax 51(4):397–402
27. Jeong YJ, Lee KS (2008) Pulmonary tuberculosis: up-to-date imaging and management. AJR Am J Roentgenol 191(3):834–844
28. Feng B, Chen X, Chen Y et al (2020) Radiomics nomogram for preoperative differentiation of lung tuberculoma from adenocarcinoma in solitary pulmonary solid nodule. Eur J Radiol 128:109022. https://doi.org/10.1016/j.ejrad.2020.109022
29. Hu Y, Zhao X, Zhang J, Han J, Dai M (2021) Value of 18F-FDG PET/CT radiomic features to distinguish solitary lung adenocarcinoma from tuberculosis. Eur J Nucl Med Mol Imaging 48(1):231–240
30. Du D, Gu J, Chen X et al (2021) Integration of PET/CT radiomics and semantic features for differentiation between active pulmonary tuberculosis and lung cancer. Mol Imaging Biol 23(2):287–298
31. Li Y, Wang B, Wen L et al (2023) Machine learning and radiomics for the prediction of multidrug resistance in cavitary pulmonary tuberculosis: a multicentre study. Eur Radiol 33(1):391–400